

Spinodal phase decomposition with dissipative fluid dynamics

Jørgen Randrup^{1,*}

¹*Nuclear Science Division, Lawrence Berkeley Laboratory, Berkeley, California , USA*

The spinodal amplification of density fluctuations is treated perturbatively within dissipative fluid dynamics including not only shear and bulk viscosity but also heat conduction, as well as a gradient term in the local pressure. The degree of spinodal amplification is calculated along specific dynamical phase trajectories and the results suggest that the effect can be greatly enhanced by tuning the collision energy so that maximum compression occurs inside the region of spinodal instability.

1. INTRODUCTION

It is expected that the confined and deconfined phases of strongly interacting matter may coexist at net baryon densities above a certain critical value and significant experimental efforts are underway to search for evidence of the associated first-order phase transition and its critical end point: a systematic beam-energy scan is currently being performed at RHIC (BNL) to look for the critical point [1]; the CBM experiment at FAIR (GSI) will study baryon-dense matter and search for the phase transition [2]; and the proposed NICA (JINR) aims at exploring the mixed phase [3].

We focus here on the possibility that the mechanism of spinodal phase decomposition may have effects that could be exploited as signals of the phase transition. Spinodal decomposition is a well-known generic phenomenon associated with first-order phase transitions that has been studied in a variety of substances and also found industrial application [4]. Furthermore, nuclear spinodal fragmentation [5] was observed in nuclear collisions at intermediate energies [6] several years ago. The present discussion is merely a brief summary of recent work [7] and a fuller exposition can be found in the literature.

* Electronic address: JRandrup@LBL.gov

2. ANALYSIS FRAMEWORK

The key parts of the framework for the analysis are described below.

2.1. Thermodynamic phase structure

The present study requires an equation of state of strongly interacting matter that displays the expected phase structure. Although significant progress has been made in understanding the thermodynamical properties of each of the phases separately, our current understanding of the phase coexistence region is not yet on firm ground. We have therefore employed a conceptually simple approximate equation of state which suffices for our present explorations.

For this purpose, we approximate the confined phase by an ideal gas of nucleons and pions augmented by a density-dependent interaction energy, while the deconfined phase is taken as an ideal gas of quarks and gluons with their interactions described by a bag constant. Fig. 1 illustrates how such two different phases may coexist thermodynamically.

The desired phase structure is then generated by suitable interpolation between those two pure phases [7] and the resulting phase diagram is shown in Fig. 2.

2.2. Transport coefficients

It is convenient to employ dissipative fluid dynamics for our dynamical studies because the specific microscopic structure of the matter under consideration enters only via the equation of state and a few transport coefficients.

The deviation of the dynamical evolution from that of an ideal fluid is governed by three transport coefficients: the shear viscosity η and the bulk viscosity ζ (which here enter only through the effective viscosity $\xi \equiv \frac{4}{3}\eta + \zeta$) as well as the heat conductivity κ . Neither their magnitudes nor their dependencies on the environment (through ρ and T) are very well known. We shall therefore employ simple parametrizations of their functional form and introduce one adjustable overall strength parameter for each one, thus enabling us to conveniently explore a range of physical scenarios. Thus, following Ref. [7], we ignore ζ and write

$$\eta(\rho, T) \doteq \eta_0 \frac{c_0}{c} d(\rho, T) h(\rho, T) , \quad (1)$$

$$\kappa(\rho, T) \doteq \kappa_0 c_0 c d(\rho, T) c_v(\rho, T) , \quad (2)$$

where $d \equiv 1/n^{1/3}$ is the interparticle spacing [8], h is the enthalpy density, and c_v is the specific heat; the conversion constant c_0 is given by

$$c_0 \equiv \frac{1}{4\pi} \left[(g_g + \frac{4}{3}g_q) \frac{\zeta(3)}{\pi^2} \right]^{\frac{1}{3}} \approx 0.12779 . \quad (3)$$

The adjustable parameters η_0 and κ_0 govern the overall magnitudes and they are expected to be at least unity.

While these approximate expressions for the transport coefficients are likely not quantitatively accurate, they are expected to approximately reflect the dependence on density and temperature. They will therefore serve well for exploring the effect of the dissipative mechanisms on the spinodal decomposition.

2.3. Dissipative fluid dynamics

We consider the early evolution of small deviations from uniformity and assume that these are planar and harmonic, $\rho(\mathbf{r}, t) = \rho_0 + \rho_k \exp(ikx - i\omega t)$ with $\delta \equiv |\rho_k|/\rho_0 \ll 1$, and similarly for the other quantities. We may then ignore terms of order $\mathcal{O}(\delta^2)$ and higher. It follows that the associated flow velocities are small, $v \ll 1$ since $\mathcal{O}(v) = \mathcal{O}(\delta)$, and thus we have $\gamma \equiv [1 - v^2]^{-1/2} = 1 + \mathcal{O}(\delta^2) \approx 1$.

It is convenient to work in the Eckart frame, where the energy-momentum tensor is

$$T^{\mu\nu} = \varepsilon u^\mu u^\nu - p \Delta^{\mu\nu} + \pi^{\mu\nu} - \Pi \Delta^{\mu\nu} . \quad (4)$$

Here $\varepsilon = u_\mu T^{\mu\nu} u_\nu$ is the energy density in the local flow frame and $p + \Pi = -\frac{1}{3} \Delta_{\mu\nu} T^{\mu\nu}$ is the sum of the local isotropic pressure p and the pressure induced by the bulk viscosity which enters through the bulk pressure,

$$\Pi = -\zeta \nabla_\mu u^\mu \approx -\zeta \nabla_i v^i = -\zeta \partial_i v^i = -\zeta \nabla \mathbf{v} . \quad (5)$$

Furthermore, the heat flow is $q^\mu = u_\nu T^{\nu\lambda} \Delta_\lambda^\mu$, while the shear viscosity enters via the stress tensor $\pi^{\mu\nu}$. In the present scenario, only the 3×3 spatial part π is non-vanishing,

$$\pi^{ij} \approx -\eta [\partial_i v^j + \partial_j v^i - \frac{1}{3} \delta_{ij} \partial_k v^k] . \quad (6)$$

Consequently, for small deviations from uniformity, we then have

$$\nabla \mathbf{T} \approx \nabla p - \eta \Delta \mathbf{v} - [\frac{1}{3} \eta + \zeta] \nabla (\nabla \mathbf{v}) . \quad (7)$$

It is interesting to note that the above result implies that isotropic expansions in N dimensions are sensitive only to the *effective* viscosity $\xi \equiv \frac{4}{3}\eta + \zeta$. To see this, assume that $\rho(\mathbf{r}) = \rho(r)$ and $\mathbf{v}(\mathbf{r}) = v(r)\hat{\mathbf{r}}$ and evaluate the viscous term in the Euler equation by use of spherical coordinates,

$$\eta\Delta\mathbf{v} + [\frac{1}{3}\eta + \zeta]\nabla(\nabla\mathbf{v}) = [\frac{4}{3}\eta + \zeta]\hat{\mathbf{r}}\partial_r\frac{1}{r^{N-1}}\partial_r r^{N-1}v. \quad (8)$$

It follows that a Hubble-type expansion, $v(r) \sim r$, is dissipation free in any dimension. Furthermore, one may expect that any expansion will seek to approach a Hubble form in order to eliminate the dissipation, so the Hubble expansion is a dynamical attractor.

The fluid-dynamic equations of motion reflect the conservation of (baryon) charge, momentum, and energy. We are interested in the dynamics of small deviations from uniformity in a semi-infinite configuration and we focus on harmonic disturbances.

The conservation of charge is ensured by the continuity equation, $\partial_\mu N^\mu \doteq 0$, which here becomes

$$C : \partial_t\rho \doteq -\rho_0\partial_x v \Rightarrow \omega\rho_k \doteq \rho_0 k v_k. \quad (9)$$

It serves to eliminate the flow velocity, $v_k = \omega\rho_k/(\rho_0 k)$. The momentum equation simplifies considerably for the present scenario of small disturbances,

$$M : h_0\partial_t v \doteq -\partial_x[p - \zeta\partial_x v] - \partial_x\pi_{xx} - \partial_t q, \quad (10)$$

where $h_0 = p_0 + \varepsilon_0$ is the enthalpy density of the uniform system and the heat flow is $\mathbf{q} = (q, 0, 0)$ (see below). The equation for energy conservation is similarly simplified,

$$E : \partial_t\varepsilon \doteq -h_0\partial_x v - \partial_x q. \quad (11)$$

By combining these latter two equations, (10) and (11), one obtains the sound equation,

$$\partial_t E - \partial_x M : \partial_t^2\varepsilon \doteq \partial_x^2\Delta[p - \zeta\partial_x v] + \partial_x^2\pi_{xx}, \quad (12)$$

which amounts to $\omega^2\varepsilon_k \doteq k^2 p_k - i\xi(\omega/\rho_0)k^2\rho_k$, where we recall that $\xi \equiv \frac{4}{3}\eta + \zeta$.

It is essential to take account of finite-range effects, without which the spinodal growth rate would become ever larger as the wave number is increased [9]. Following Ref. [10], we introduce a gradient correction in the equation of state. To leading order in the disturbance amplitudes, the effect of the gradient term on the local pressure is given by

$$p(\mathbf{r}) \approx p_0(\varepsilon(\mathbf{r}), \rho(\mathbf{r})) - C\rho_0\nabla^2\rho(\mathbf{r}), \quad (13)$$

where $p_0(\varepsilon, \rho)$ is the microcanonical equation of state, i.e. the pressure in uniform matter having the specified energy and charge densities. The pressure amplitude is then modified accordingly, $p_k \rightarrow p_k + C\rho_0 k^2 \rho_k$.

With the above preparations, it is then possible to derive the dispersion equation for the collective frequency, with viscosity, heat conductivity, and finite-range effects included,

$$\omega^2 \doteq v_T^2 k^2 + C \frac{\rho_0^2}{h_0} k^4 - i\xi \frac{\omega}{h_0} k^2 + \frac{v_s^2 - v_T^2}{1 + i\kappa k^2 / \omega c_v} k^2. \quad (14)$$

Apart from the addition of the finite-range term, it agrees with the one used in Ref. [11].

3. RESULTS

We now briefly discuss the main results of the analysis.

3.1. Dispersion relation

Fig. 3 illustrates this dispersion relation for thermodynamic scenarios relevant to the present study. Selecting a phase point in the central region of the phase coexistence region where both the isothermal and the isentropic sound velocities are imaginary, we consider the growth rate γ as a function of the wave number k of the density undulation being amplified. The non-dissipative treatment with ideal finite-range fluid dynamics provides a convenient reference result.

Relative to this reference, the inclusion of viscosity slows the growth but does *not* change the domain of instability which is still delineated by the vanishing of the isentropic sound speed v_s . We see that the inclusion of a minimal amount of viscosity ($\eta_0 = 1$) leads to a significant reduction in γ and also shifts the optimal length scale towards larger values.

On the other hand, relative to the ideal scenario, the inclusion of heat conductivity enlarges the domain of instability, the boundary being now determined by the vanishing of the isothermal sound speed v_T . Thus, generally, the inclusion of heat conductivity increases the growth rates, particularly at the high end of the unstable k range.

While the inclusion of both minimal viscosity and minimal heat conduction necessarily enlarges the unstable k range, it does somewhat reduce the fastest growth rates. However, it hardly affects the scale of the fastest-growing modes, k_{\max} . As the strengths of the dissipative

terms are further increased, the growth rate γ_k decreases steadily and, at the same time, the maximum in the dispersion relation moves gradually downwards in k .

3.2. Dynamical evolution

It is possible to obtain semi-quantitative estimates of the dynamical phase trajectories, $(\rho(t), T(t))$, on the basis of the results presented in Ref. [12] which used a number of different dynamical models to extract the time evolution of the net baryon density, $\rho(t)$, and the energy density, $\varepsilon(t)$, in the center of a head-on gold-gold collision for the range of collision energies anticipated at FAIR. Here we employ phase trajectories extracted from calculations with the 3-fluid model [13] and UrQMD [14] at beam kinetic energies of 5 AGeV, shown in Fig. 4.

Once $\rho(t)$ and $T(t)$ have been specified, the time evolution of the collective frequency can be obtained by use of the dispersion equation (14) and it is then possible to calculate the degree of amplification experienced by the mode, as illustrated in Fig. 5. The evolution of the amplitude of a mode ν having the complex frequency $\omega_\nu = \epsilon_\nu + i\gamma_\nu$ is governed by the equation

$$\frac{d}{dt}A_\nu(t) = -i\omega_\nu A_\nu(t) + B_\nu(t) , \quad (15)$$

where the last term represents the dissipative coupling to the environment which is assumed to be Markovian, $\langle B_\nu(t)B_\mu(t')^* \rangle = 2\mathcal{D}_{\nu\mu}\delta(t-t')$ [15]. The equal-time correlation function, $\sigma_{\nu\mu}(t) = \langle A_\nu(t)A_\mu(t)^* \rangle$ then evolves according to the Lalime equation [15],

$$\frac{d}{dt}\sigma_{\nu\mu}(t) = 2\mathcal{D}_{\nu\mu}(t) - i[\omega_\nu(t) - \omega_\mu(t)^*]\sigma_{\nu\mu}(t) . \quad (16)$$

We are particularly interested in the time evolution of the diagonal components of the covariance matrix, $\sigma_{\nu\nu} = \sigma_\nu^2$, which are given by

$$\sigma_\nu^2(t) = \left[\sigma_\nu^2(t_i) + \int_{t_i}^t 2\mathcal{D}_{\nu\nu}(t') e^{-2\Gamma_\nu(t')} dt' \right] e^{2\Gamma_\nu(t)} . \quad (17)$$

The degree of amplification achieved is thus governed by the *amplification coefficient*,

$$\Gamma_\nu(t) \equiv \int_{t_i}^t \text{Im}[\omega_\nu(t')] dt' = \int_{t_i}^t \gamma_\nu(t') dt' , \quad (18)$$

which depends strongly on the length of time spent in the phase region of spinodal instability.

This is illustrated in Fig. 6 which shows $G_k \equiv \exp(\Gamma_k)$, the degree of amplitude growth obtained for the entire range of wave numbers, as obtained with various degrees of dissipation.

While we concentrate on the phase trajectory that reaches its maximum compression inside the spinodal region (the one based on the 3-fluid model results for 5 AGeV), we also show the result of a more penetrating trajectory to bring out the importance of adjusting the collision energy for optimal effect.

In addition to the result of ideal fluid dynamics, we show results for various degrees of dissipation, ranging from minimal, i.e. $(\eta_0, \kappa_0) = (1, 1)$, to five times that. While viscosity generally slows the evolution, thus also suppressing the growth of instabilities, heat conductivity generally increases the growth rate. The combined effect of introducing small amounts of dissipation then tends to enhance the amplification. Thus the resulting degree of non-uniformity is fairly robust against moderate changes in the dissipation strength and, consequently, our conclusions do not appear to be sensitive to the specific parametrizations of the transport coefficients.

The results displayed in Fig. 6 bring out the characteristic feature of spinodal instability, namely that the amplification mechanism favors certain length scales. We note that the two-point correlation coefficient σ_k^2 is proportional to G_k^2 and thus exhibits a stronger peaking. More generally, since the N -point correlation is proportional to G_k^N , the spinodal effect manifests itself progressively stronger in the higher-order correlations.

The nuclear liquid-gas phase transition could be revealed by the unique signal of equal-size intermediate-mass fragments in each event [6]. The studies summarized above suggest that if the equation of state has a form that admits spinodal instability, then the conditions during a nuclear collision at suitably adjusted energies may allow the development of significant clumping which in turn might lead to visible signals. Of course, the confinement transition is inherently more difficult to investigate experimentally because any plasma drops that may have been formed will ultimately hadronize and are thus harder to identify. Nevertheless, the transient existence of spatially separated blobs of deconfined matter might be revealed by careful examination of suitable multi-particle correlations [17–19].

Finally, it should be stressed that the above analysis rests on the assumption that the phase structure is of the familiar Van-der-Waals form characterizing the liquid-gas transition, for which spinodal decomposition is an accompanying phenomenon. However, as pointed out by Iosilevskiy [20], the T - p representation of the plasma-hadron coexistence looks qualitatively different from that of a liquid-gas system and the phase transformation may therefore proceed differently. This important possibility awaits further exploration.

ACKNOWLEDGMENTS

We wish to acknowledge helpful discussions with I. L. Iosilevskiy, V. Koch, J. Liao, H. C. Song, and D. N. Voskresensky. This work was supported by the Director, Office of Energy Research, Office of High Energy and Nuclear Physics, Nuclear Physics Division of the U.S. Department of Energy under Contract No. DE-AC02-05CH11231.

-
1. B. I. Abelev *et al.*, Internal STAR Note SN0493, 2009:
<http://drupal.star.bnl.gov/STAR/starnotes/public/sn0493>.
 2. B. Friman *et al.*, *The CBM Physics Book*, Springer, Berlin, 2010, in press.
 3. A. N. Sissakian and A. S. Sorin, *J. Phys. G* **36**, 064069 (2009).
 4. R. A. L. Jones, *Soft Condensed Matter*, Oxford University Press, Oxford, 2002.
 5. Ph. Chomaz, M. Colonna, and J. Randrup, *Phys. Rep.* **389**, 263 (2004).
 6. B. Borderie *et al.*, *Phys. Rev. Lett.* **86**, 3252 (2001).
 7. J. Randrup, *Phys. Rev. C* **82**, 034902 (2010).
 8. J. Liao and V. Koch, *Phys. Rev. C* **81**, 014902 (2010).
 9. J. Randrup, *Phys. Rev. Lett.* **92**, 122301 (2004).
 10. J. Randrup, *Phys. Rev. C* **79**, 054911 (2009).
 11. H. Heiselberg, C. J. Pethick, and D. G. Ravenhall, *Ann. Phys.* **223**, 37 (1993).
 12. I. C. Arsene *et al.*, *Phys. Rev. C* **75**, 034902 (2007).
 13. Yu. B. Ivanov, V. N. Russkikh, and V. D. Toneev, *Phys. Rev. C* **73**, 044904 (2006).
 14. S. A. Bass *et al.*, *Prog. Part. Nucl. Phys.* **41**, 225 (1998); M. Bleicher *et al.*, *J. Phys. G* **25**, 1859 (1999).
 15. M. Colonna, Ph. Chomaz, and J. Randrup, *Nucl. Phys. A* **567**, 637 (1994).
 16. J. Randrup and J. Cleymans, *Phys. Rev. C* **74**, 047901 (2006).
 17. D. Bower and S. Gavin, *Phys. Rev. C* **64**, 051902 (2001).
 18. J. Randrup, *Acta Phys. Hung. A* **22**, 69 (2005).
 19. V. Koch, A. Majumder, and J. Randrup, *Phys. Rev. C* **72**, 064903 (2005).
 20. Comment made by I. L. Iosilevskiy during the discussion.

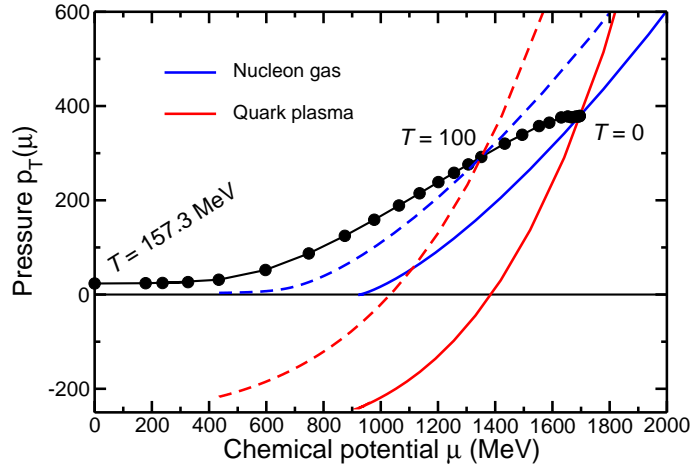


Figure 1. Phase crossing: The pressures in the two idealized phases are shown as functions of the chemical potential μ for $T = 0$ (solid) and $T = 100$ MeV (dashed); the systems are in mutual thermodynamic equilibrium at the μ value for which the two curves cross. The crossing points obtained by this procedure for various T are connected by the solid curve that terminates at $T_{\text{max}} \approx 156.4$ MeV; above this T the plasma is thermodynamically favorable at all μ .

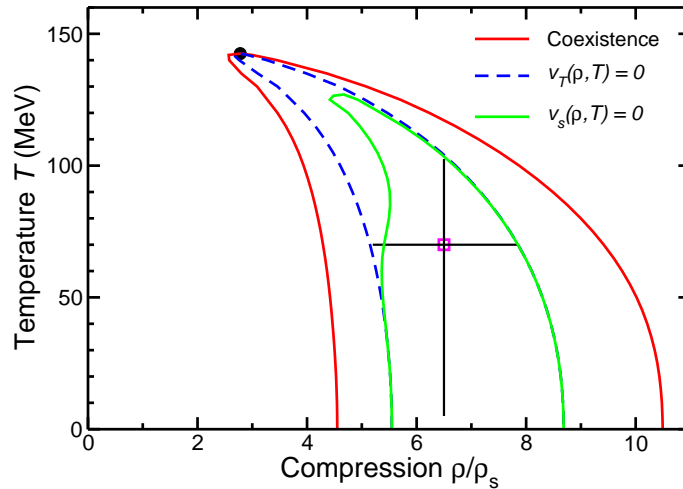


Figure 2. Phase diagram: The crossing points for the two idealized phases (see Fig. 1) in the ρ - T phase plane (dot-dashed curves) and the phase coexistence boundary (outer solid) obtained by interpolating between those two idealized phases. Also shown are the isothermal spinodal where $v_T = 0$ (dashed), and the isentropic spinodal where $v_s = 0$ (inner solid), together with the critical point. The dispersion relation shown in Fig. 3 was calculated at the square.

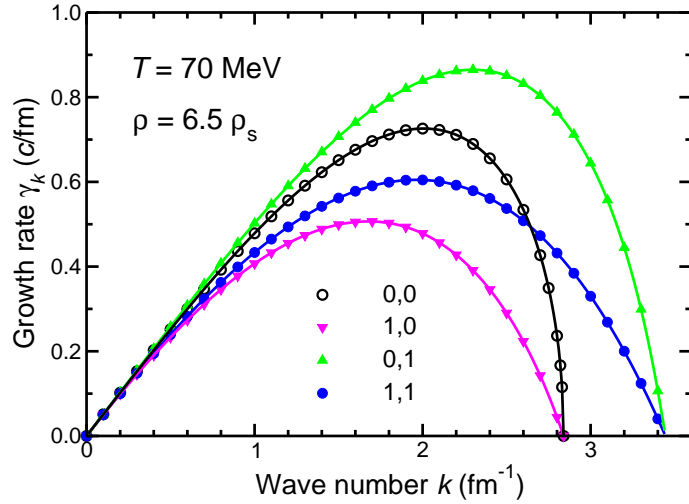


Figure 3. The growth rate $\gamma_k(\rho, T)$, as a function of the wave number k , calculated with finite-range fluid dynamics at $\rho = 6.5 \rho_s$ and $T = 70$ MeV for four different combinations of dissipation: no dissipation ($\eta_0 = 0, \kappa_0 = 0$); minimal viscosity but no heat conduction ($\eta_0 = 1, \kappa_0 = 0$); no viscosity but minimal heat conduction ($\eta_0 = 0, \kappa_0 = 1$); both minimal viscosity and minimal heat conduction ($\eta_0 = 1, \kappa_0 = 1$).

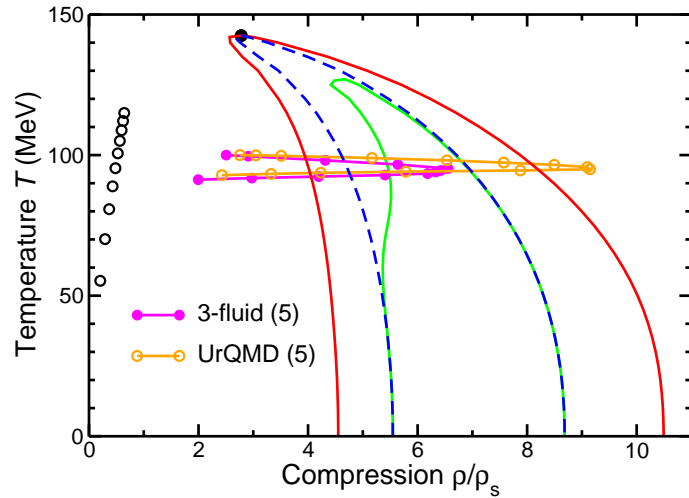


Figure 4. Dynamical phase trajectories based on the 3-fluid and UrQMD density evolutions obtained for 5 AGeV in Ref. [12]; the associated time-dependent growth rates $\gamma_k(t)$ are illustrated in Fig. 5. The symbols along the trajectories are equidistant in time with $\Delta t = 1$ fm/c, while the open dots on the left indicate the freezeout locations for bombarding energies of $E = 1, \dots, 10$ AGeV obtained from fits to experimental data as discussed in Ref. [16].

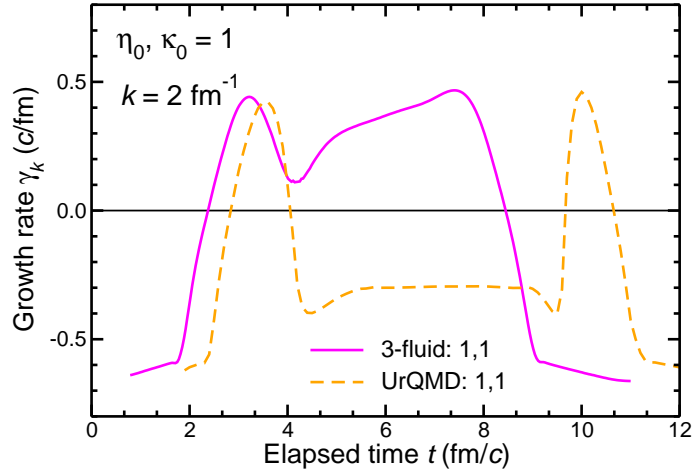


Figure 5. The spinodal growth rate $\gamma_{\mathbf{k}}(t) = \text{Re}[\omega_{\mathbf{k}}(t)]$ for modes with $k = 2 \text{ fm}^{-1}$, calculated with minimal dissipation along the two dynamical (ρ, T) phase trajectories shown in Fig. 4.

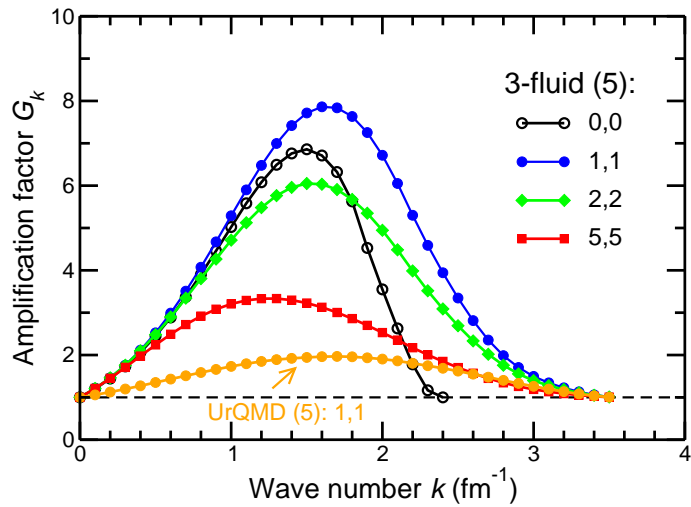


Figure 6. As a function of the wave number k is shown the amplification factor $G_k = \exp(\Gamma_k)$ resulting from motion along the 3-fluid phase trajectory displayed in Fig. 4 for various degrees of dissipation (indicated by the values of η_0 and κ_0). Also shown is the result for the UrQMD trajectory in Fig. 4 using minimal dissipation, *i.e.* $(\eta_0, \kappa_0) = (1, 1)$.

FIGURE CAPTIONS

- Fig. 1: Phase crossing: The pressures in the two idealized phases are shown as functions of the chemical potential μ for $T = 0$ (solid) and $T = 100$ MeV (dashed); the systems are in mutual thermodynamic equilibrium at the μ value for which the two curves cross. The crossing points obtained by this procedure for various T are connected by the solid curve that terminates at $T_{\text{max}} \approx 156.4$ MeV; above this T the plasma is thermodynamically favorable at all μ .
- Fig. 2: Phase diagram: The crossing points for the two idealized phases (see Fig. 1) in the ρ - T phase plane (dot-dashed curves) and the phase coexistence boundary (outer solid) obtained by interpolating between those two idealized phases. Also shown are the isothermal spinodal where $v_T = 0$ (dashed), and the isentropic spinodal where $v_s = 0$ (inner solid), together with the critical point. The dispersion relation shown in Fig. 3 was calculated at the square.
- Fig. 3: The growth rate $\gamma_k(\rho, T)$, as a function of the wave number k , calculated with finite-range fluid dynamics at $\rho = 6.5 \rho_s$ and $T = 70$ MeV for four different combinations of dissipation: no dissipation ($\eta_0 = 0, \kappa_0 = 0$); minimal viscosity but no heat conduction ($\eta_0 = 1, \kappa_0 = 0$); no viscosity but minimal heat conduction ($\eta_0 = 0, \kappa_0 = 1$); both minimal viscosity and minimal heat conduction ($\eta_0 = 1, \kappa_0 = 1$).
- Fig. 4: Dynamical phase trajectories based on the 3-fluid and UrQMD density evolutions obtained for 5 AGeV in Ref. [12]; the associated time-dependent growth rates $\gamma_{\mathbf{k}}(t)$ are illustrated in Fig. 5. The symbols along the trajectories are equidistant in time with $\Delta t = 1$ fm/ c , while the open dots on the left indicate the freezeout locations for bombarding energies of $E = 1, \dots, 10$ AGeV obtained from fits to experimental data as discussed in Ref. [16].
- Fig. 5: The spinodal growth rate $\gamma_{\mathbf{k}}(t) = \text{Re}[\omega_{\mathbf{k}}(t)]$ for modes with $k = 2$ fm $^{-1}$, calculated with minimal dissipation along the two dynamical (ρ, T) phase trajectories shown in Fig. 4.
- Fig. 6: As a function of the wave number k is shown the amplification factor $G_k = \exp(\Gamma_k)$ resulting from motion along the 3-fluid phase trajectory displayed in Fig. 4 for various

degrees of dissipation (indicated by the values of η_0 and κ_0). Also shown is the result for the UrQMD trajectory in Fig. 4 using minimal dissipation, *i.e.* $(\eta_0, \kappa_0) = (1, 1)$.